Applied Radiation and Isotopes 166 (2020) 109422

Contents lists available at ScienceDirect

Applied Radiation and Isotopes

journal homepage: http://www.elsevier.com/locate/apradiso

The neutron component of background of an HPGe detector operating in a surface laboratory

M. Baginova [a,b,*], P. Vojtyla [a], P.P. Povinec [b]

[a] CERN, Geneva, 1211, Switzerland
[b] Faculty of Mathematics, Physics and Informatics, Comenius University, 842 48, Bratislava, Slovakia

ARTICLE INFO

Keywords:
Monte Carlo simulation
Neutron induced background
GEANT4
High-purity Ge detector

ABSTRACT

Investigation of neutron-induced background was carried out by studying interactions of cosmic-ray neutrons with an HPGe detector inside its shield placed on a ground floor of a 3-storey building. The study was conducted experimentally and by Monte Carlo simulations using GEANT4 simulation tool. Detailed analysis of measured background γ-ray spectra showed that many γ-lines visible in the spectra were induced by neutrons. The majority of detected γ-rays originated in germanium, copper, lead and tin. Iron and aluminium components were less important background sources. Inelastic scattering and neutron capture were the most often occurring processes of neutron interactions with the detector and its shielding. The contamination by natural radionuclides, specifically of ^{40}K, ^{214}Pb, ^{214}Bi and ^{208}Tl, was also present in the background spectra. Nevertheless, approximately 35% of ^{208}Tl peak at the energy of 2614.51 keV was produced by inelastic scattering of neutrons on ^{208}Pb nuclei. The experimental background was compared with GEANT4 simulations, which were carried out without and with the shielding layer of the building. The final integral counting rates for measured spectrum in the energy range from 50 keV to 2875 keV was 1.26 ± 0.07 s^{-1} and for simulated one 1.25 ± 0.13 s^{-1}, indicating very good agreement with the experiment.

1. Introduction

High-purity germanium (HPGe) detectors have been very often used for analysis of radionuclides at very low levels, as well as in experiments looking for rare events, especially those operating in deep underground laboratories. Success of such experiments depends mainly on the detector background that can overlap the useful signal coming from the detector. For this reason, it is very important to know all sources of background of HPGe detectors and minimize or eliminate their influence on the searched signals. A significant source of the Ge detector background has been due to neutrons. Neutrons interacting with the HPGe detector materials and the shield produces many γ-rays that can hide or imitate the searched signal (Kudryavtsev et al., 2008). Neutrons are present not only in surface laboratories but also in deep underground laboratories, either as a result of spontaneous fission of natural long-lived radionuclides, (α, n) reactions, or muon interactions with surrounding rocks and detector materials (Baginova et al., 2018).

Reliable identification and investigation of neutron-induced background is a challenge due to diversity of neutron interactions with detectors and shielding materials. There are several studies dealing with neutron induced background of Ge detectors focusing mainly on neutron interactions with Ge nuclei (e.g. Jovancevic et al., 2010; Chao, 1993). Neutrons interacting with Ge crystals produce several γ-lines resulting from capture of thermal neutrons and inelastic scattering of fast neutrons on individual Ge nuclei. These γ-lines can be used for estimation of the flux of thermal and fast neutrons around a detector. Different types of Ge detectors and various shielding materials were used for background measurements. It has been found out that the production of neutrons induced by cosmic muons significantly depends on the atomic number Z of the shielding material, as it increases with rising Z. Therefore, a shield with high Z, which is commonly used for reduction of γ-rays coming from natural radionuclides and from interactions of cosmic rays is a source of neutrons, too (Jovancevic et al., 2010). This has to be taken into account especially when building large shields for surface laboratories, compromising the composition and thickness of the shield (Povinec et al., 2008).

Germanium γ-ray peaks were used for identification of neutron sources in the Ge detector environments, as well as for calculation of their contribution to detector background. It was found that the germanium crystal itself is one of the most intensive sources of neutron-

* Corresponding author. CERN, Geneva, 1211, Switzerland.
E-mail address: miloslava.baginova@cern.ch (M. Baginova).

https://doi.org/10.1016/j.apradiso.2020.109422
Received 31 October 2019; Received in revised form 12 April 2020; Accepted 9 September 2020
Available online 16 September 2020

induced γ-rays in an HPGe detector (Chao, 1993).

However, a study providing complex information on the neutron induced background in Ge spectrometers is still missing. In order to bring additional information about the neutron-induced background and to contribute to better understanding of low-background detector systems, γ-ray background of an HPGe detector operating in a surface laboratory was measured and compared with Monte Carlo simulations in the present study. The knowledge obtained in (Baginova et al., 2018) provided useful hints for this work.

2. Cosmic rays at the sea level

Background of low-level Ge detectors operating in surface laboratories is mainly caused by secondary cosmic rays, radioactive contamination of materials used for construction of detectors and their shields, and by decay products of radon. Interactions of primary high-energy cosmic ray particles with atmospheric nuclei produce secondary particles, which interact further in the atmosphere producing next generations of particle cascades. The ability of a particle to reach sea level depends on the particle type, energy, zenith angle of propagation and mean lifetime at rest. Cosmic rays at sea level consist of hadrons, electrons, γ-rays, muons, nuclei and antinucleons with energy up to a few TeV. These particles form at sea level soft, nucleonic and hard components of cosmic rays. Electrons, positrons and γ-rays belong to the soft component. The nucleonic component consists mainly of protons and neutrons, and the hard component contains mostly muons. The hard component is dominant at the sea level, as the most numerous particles at the sea level are muons with abundance of about 63%. The second most abundant particles are neutrons with occurrence of about 21% and the third numerous particles are electrons, positrons and γ-rays with abundance of about 15%. The rest, about 1% of cosmic rays at the sea level is formed by protons, pions and nuclei (Greider, 2001; Bogdanova et al., 2006).

Although muons are the dominant particle type at the sea level, we can reduce their effect by operating detectors deep underground where muon fluxes are lower by several orders of magnitude. In surface laboratories we may apply anti-cosmic (anti-coincidence) pulse-rejection techniques. Therefore, the most difficult cosmic-ray component to deal with are neutrons, as the fluxes of protons, the second part of the nucleonic component, are very small.

3. Neutron cross sections

Neutrons interact with matter by different processes depending on their energy and material cross sections. Slow and thermal neutrons interact by neutron capture, while fast neutrons interact by elastic and inelastic scattering. Neutron cross sections for individual isotopes forming the materials of Ge detector and the shield are very important for investigation of neutron induced background. Isotopes with large cross sections, such as isotopes of lead and copper, interact with neutrons easily so that they can significantly contribute to the neutron background. Lead and copper are materials frequently used in certain parts of HPGe detectors. The crystal holder is usually made of copper, as well as the internal part of the shield is covered with a copper layer. Lead is almost always the largest part of the detector shield. Usually, lead is one of the most frequently used material for construction of massive shields for HPGe detectors operating deep underground. The amount of lead in a shield of an HPGe detector commonly used in a surface laboratory is around 1 ton. Therefore, due to its high cross sections and mass, the shield is a significant contributor to the neutron background.

Lead as an element consists of four naturally occurring isotopes: ^{204}Pb (1.4%), ^{206}Pb (24.1%), ^{207}Pb (22.1%), and ^{208}Pb (52.4%). Copper has two naturally occurring isotopes, ^{63}Cu and ^{65}Cu, with abundances of 69.15% and 30.85%, respectively. The cross sections for individual lead and copper isotopes for interactions with neutrons are shown in Fig. 1.

Quantitative parameters of cross sections of individual isotopes were compared and following was found. For all four lead isotopes the elastic scattering significantly dominates until the resonance region, which can be split into two parts. The first part is characterized by sharp fluctuations of cross sections for both, neutron capture and elastic scattering. In the second part, the elastic scattering dominates, and the cross sections fluctuate with decreasing amplitude.

For ^{204}Pb, the resonance region opens at 3.7 keV and ranges up to 1.8 MeV. Within the first part of the region up to about 75 keV, the neutron capture and elastic scattering are equally probable. Beyond the resonance region, the elastic scattering gains significance again. The channel of inelastic scattering opens at about 200 keV and drops sharply beyond 10 MeV. In the energy region of 1.8–10 MeV, elastic and inelastic scattering concur. Nevertheless, around 8–9 MeV, the inelastic scattering is more probable.

For ^{206}Pb, the resonance region extends from about 3 keV to 2.5 MeV. In the first part of the region up to about 820 keV, the elastic scattering gradually takes over. In the energy region of 8–9 MeV, elastic and inelastic scattering are equally probable.

For ^{207}Pb, the resonance region is wider and ranges from about 3 keV to 4.5 MeV. In the first part of the region, up to about 680 keV, the elastic scattering clearly outweighs. In the second part of the resonance region, the inelastic scattering cross section increases quickly. The elastic and inelastic scattering are equally probable processes from 6.5 to 8.0 MeV.

For ^{208}Pb, the resonance region ranges from about 43 keV to 5.5 MeV, where the elastic scattering highly predominates The channel of inelastic scattering opens at 900 keV and, from 7.5 to 8.5 MeV, the elastic and inelastic scattering are equally probable.

The inelastic scattering is a significant process for all lead isotopes around the energy of 8 MeV, the binding energy per nucleon in a lead nucleus.

The behaviour of cross sections for both copper isotopes is very similar to lead isotopes.

For ^{63}Cu, the neutron capture predominates up to 19 meV. Above this energy the elastic scattering gains significance until the resonance region, which extends from about 400 eV up to 1.1 MeV. Inside the region, the neutron capture is the most probable reaction up to 1 keV. From 50 keV the elastic scattering dominates. The inelastic channel opens at 680 keV and it is equally probable as elastic scattering in the energy range of 2.5–6 MeV.

Finally, for ^{65}Cu, the elastic scattering dominates up to 230 eV, where the resonance region starts. The region ranges up to 1.1 MeV. In the region up to 50 keV, cross sections of the elastic scattering and neutron capture are comparable. Above this energy, the elastic scattering takes over. The inelastic channel opens at 780 keV and in the energy range of 3.5–5 MeV, both, the elastic and inelastic scattering are equally probable.

In the energy range of 3.5–5 MeV, neutrons interact easily by inelastic scattering with both copper isotopes. The neutron capture is the preferred process for thermal neutrons and a very probable process for slow neutrons from 400 eV to 50 keV.

4. Detector background

4.1. Experimental setup

Investigation of neutron induced-background was carried out by a study of cosmic ray interactions with an HPGe detector inside a shield. The study was conducted experimentally and by Monte Carlo simulations using the GEANT4 simulation tool developed at CERN (http://geant.cern.ch/; Agostinelli et al., 2003; Allison et al., 2006, 2016).

A Mirion Technologies (Canberra) coaxial low-level p-type HPGe detector GC-5019 with a relative efficiency of 50% was used for background measurement. The germanium crystal was a cylinder with a cavity inside the crystal. The dimensions of the crystal were 66 mm in diameter and 59 mm in height. The cavity was 10 mm in diameter and 45 mm in height. The crystal was placed in a thermoplastic foil and in a

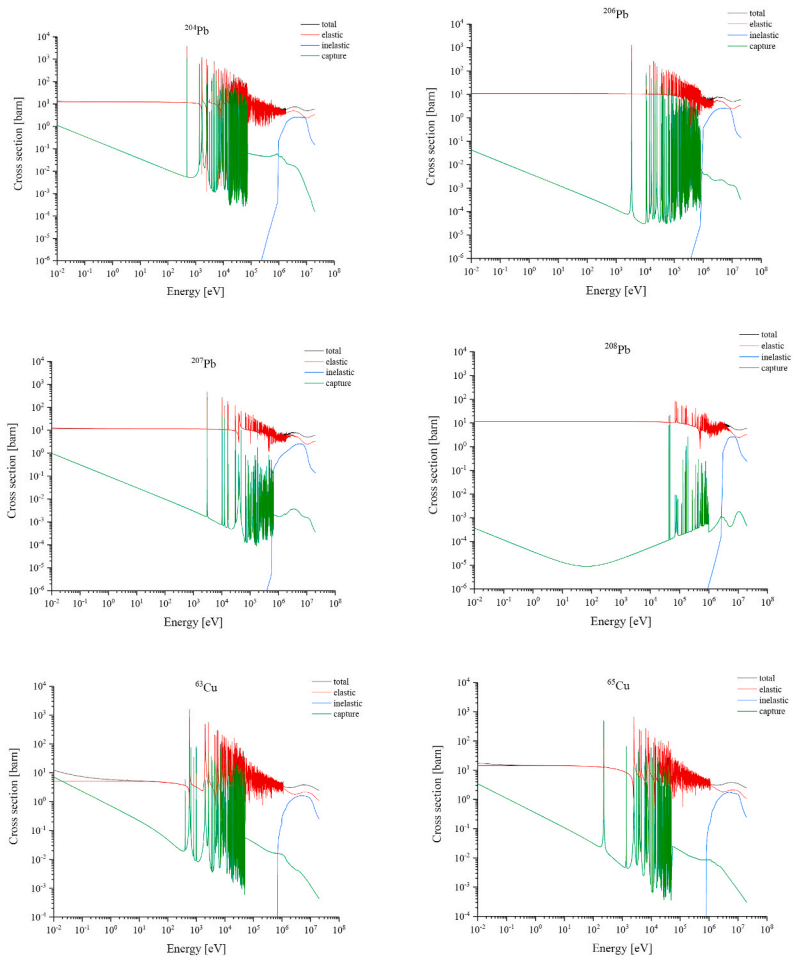

Fig. 1. Calculated cross sections for elastic and inelastic scattering and neutron capture in lead and copper isotopes. Data taken from JENDL 4.0 database (http://wwwndc.jaea.go.jp/jendl/j40/j40.html).

copper crystal holder, which was enclosed in an aluminium "swan-neck" cryostat. The detector was placed in a low-level shield consisting of (from outside to inside) 9.5 mm of carbon steel, 92 mm of common lead, 10 mm of old low-activity lead, 1 mm of tin foil, and 1.5 mm of copper cladding. The outer dimensions of the shield were 508 mm in diameter and 635 mm in height. The preamplifier was placed outside the shield. The "swan-neck" prevented a direct sight of the crystal on a Dewar vessel and the floor below. The energy resolution of the detector was 2.07 keV for 1332.40 keV γ-rays of ^{60}Co. The Canberra GENIE 2000 software was used for γ-ray spectrum analysis. The spectrum was acquired in the energy range from 10 to 3000 keV during 84 h of live time. The measurement was carried out after an experiment with an Am–Be neutron source (Baginova et al., 2018), in which two circular iron absorbers and one plastic beaker were placed above the detector with the aim of reducing the dead time by increasing the source-detector distance and absorbing the ^{241}Am gamma rays. As the same background spectrum was used in this work, the iron absorbers and the plastic beaker were left inside the shield. The setup, as it was implemented in the GEANT4 simulation code, is shown in Fig. 2a.

4.2. Monte Carlo simulations

The GEANT4 simulation code was used for Monte Carlo simulations of Ge detector background. GEANT4 is an object-oriented simulation toolkit, which provides an extensive set of software components for simulation of particle interactions with matter in a wide energy range. The code includes all aspects of the simulation process, such as the geometry, materials, particles, the tracking, physics processes and the detector response. The software is capable to generate and store events and tracks, to visualize the detector and particle trajectories, and to record the simulation data, energy deposition included. GEANT4 disposes with extensive databases of cross sections, which are stored in individual data files for specific processes (http://geant.cern.ch/; Agostinelli et al., 2003; Allison et al., 2006, 2016). The GEANT4 simulation code is equally suitable for simulations in High Energy Physics as in Low Energy Physics. The code was already validated for low background experiments, such as dark matter or neutrinoless ββ decay searches, where the precision of simulations is very important. For example, the detector geometry and its surrounding, the source particles and the background spectra were simulated by GEANT4 in underground experiments such as CRESST, COSINE, EDELWEISS or SuperNEMO (e.g. Abdelhameed et al., 2019; Adhikari et al., 2018; Armengaud et al., 2017; M. Kauer and the SuperNEMO Collaboration 2009, 2008). Nevertheless, GEANT4 is commonly used also for cosmic-ray background simulations, (e.g. Shun-Li et al., 2015; Medhat and Wang, 2014; Hung et al., 2017). In all these studies, simulations well agreed with experimentally measured spectra.

The detector and shield geometry were coded in GEANT4, including composition of shielding materials and impurities. Detailed drawings of the detector setup were provided by Mirion Technologies/Canberra for the study.

The setup was placed into a box with dimensions of $7 \times 4 \times 3$ m^3 representing the laboratory with concrete walls of 32 cm thickness. The laboratory with the HPGe detector is located in a basement of a building and the cosmic rays from an open area pass through masonry structures of the building. The detailed structure of the overhead material layers

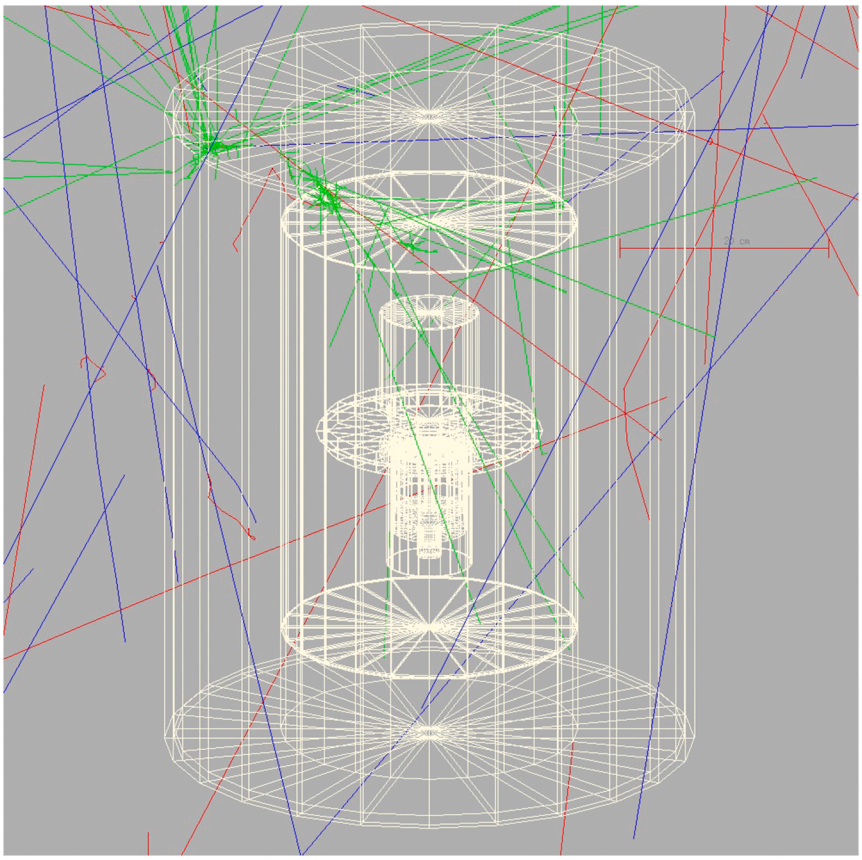

Fig. 2a. GEANT 4 simulation of the experimental setup with several simulated cosmic ray interactions (trajectories of positive particles are blue, of negative particles are red and of neutral particles are green). (For interpretation of the references to colour in this figure legend, the reader is referred to the web version of this article.)

was not known but its concrete equivalent was estimated to be 1 m, arranged as a ceiling equivalent to a roof and two floors. We expect that the nucleonic and soft components of cosmic rays were reduced approximately by a factor of 4 (Ziegler, 1996).

The cosmic rays at sea level were used as source of particles impinging on the setup, without and with the concrete overhead shielding. The source consisted of muons, neutrons, electrons, positrons, γ-rays, protons and pions. The measured energy spectra of individual cosmic ray particles taken from (Greider, 2001) were implemented into GEANT4 simulation. The intensity of particles was coded based on their abundances in cosmic rays at sea level as indicated in (Bogdanova et al., 2006). The assumed relative abundances of different particle types were: muons (63%), neutrons (21%), electrons and positrons (7.5%), γ-rays (7.5%), and protons and pions (1%). The fluxes of positive and negative muons, positive and negative pions, as well as electrons and positrons were calculated from charge ratios reported in (Greider, 2001). The cosmic-ray particle source was modelled as a plane (10×10 m^2) placed above the laboratory. See (Greider, 2001) for detailed information on spectral fluxes of the different cosmic-ray particle types.

SHIELDING 2.1 was selected as the most suitable GEANT physics list. It is an ideal choice to study neutron interactions in underground or low background experiments thanks to an appropriate composition of electromagnetic and hadronic physics processes.

The G4NDL 4.5 and G4NEUTRONXS 1.4 data files were used for neutron processes and G4EMLOW 6.5 data file for γ-ray interactions. G4NEUTRONXS 1.4 is suitable for elements with natural composition, and G4NDL 4.5 is used especially for thermal neutron cross sections.

The correct coding of the given detector and shield to GEANT4 and the software setup with the selection of the physics data files were validated in a previous work (Baginova et al., 2018). Interactions of neutrons from a ^{241}Am–Be neutron source with an HPGe detector was investigated experimentally and by Monte Carlo simulations. The integral count rates of the two spectra were compared and a good agreement was found (experiment 378 ± 3 s^{-1}, simulation 369 ± 11 s^{-1}). Count rates of many neutron induced peaks were compared, too. For example, the measured ^{65}Cu peak at the energy of 770.60 keV resulting from inelastic scattering of neutrons on Cu nuclei had a count rate of 0.1 ± 0.01 s^{-1} to be compared with the simulated one of 0.1 ± 0.03 s^{-1}. Similarly, the measured count rate of 0.31 ± 0.02 s^{-1} of the ^{207}Pb peak at the energy of 569.70 keV matched the count rate of the simulated peak 0.29 ± 0.03 s^{-1}.

5. Results and discussion

5.1. Evaluation of the experimental background γ-ray spectrum

The measured background γ-ray spectrum was analysed and evaluated in detail. To make the peaks and reaction formulas more visible, the γ-ray spectra are shown in three energy regions: 0–1 MeV (Fig. 3.), 1–2 MeV (Fig. 4.) and 2–3 MeV (Fig. 5.). Many peaks were identified and explained also using information from the previous experiment with Am–Be neutron source (Baginova et al., 2018). Different colours are used to mark peaks from different contributors. Very short-lived radionuclides (excited states with half-lives <1 ms) are marked with the asterisk.

The observed count rates depend on the particle spectral fluxes, isotope-specific nuclear-reaction cross-sections, isotope abundances, γ-ray emission probabilities and detection efficiencies. Apparently, these are complex processes to combine and could be analysed on demand by using the information provided by GEANT4 code, for example.

Triangular γ-ray peaks, which are typical for interactions of fast neutrons with individual Ge nuclei, are present in the spectra. Their

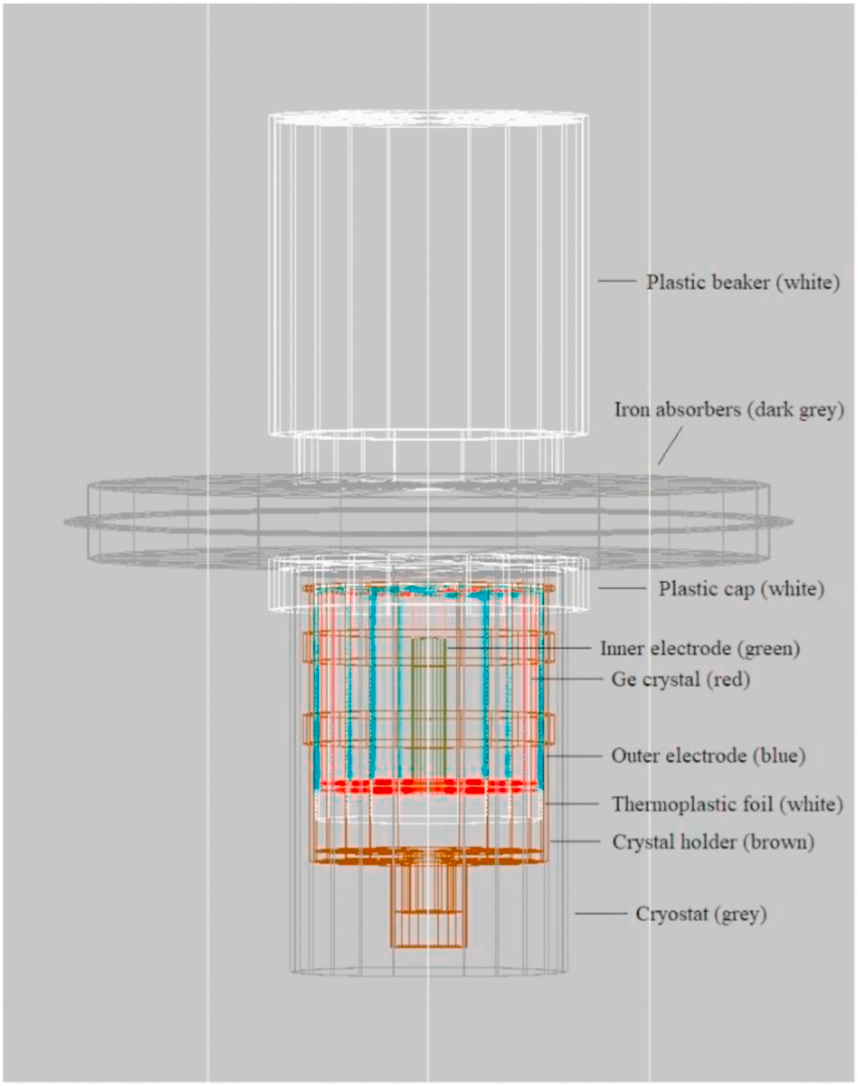

Fig. 2b. Detailed view of the experimental setup with description of the detector parts.

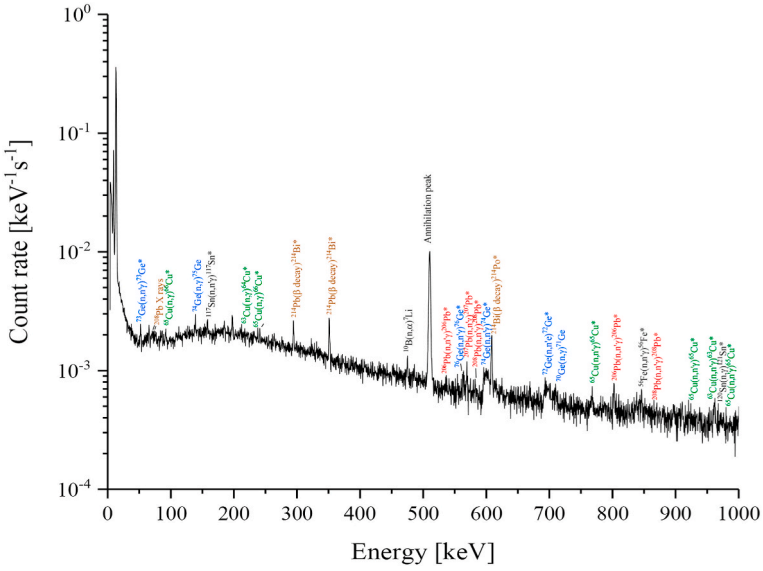

Fig. 3. Experimental HPGe detector background spectrum for energy range from 0 to 1 MeV. (Ge peaks-blue, Cu peaks-green, Pb peaks-red, contamination-brown)

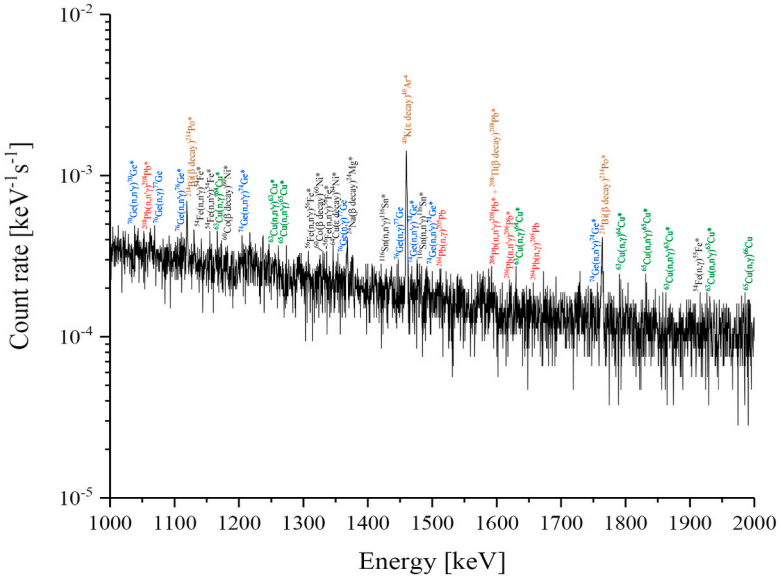

Fig. 4. Experimental HPGe detector background spectrum for energy range from 1 to 2 MeV. (Ge peaks-blue, Cu peaks-green, Pb peaks-red, contamination-brown)

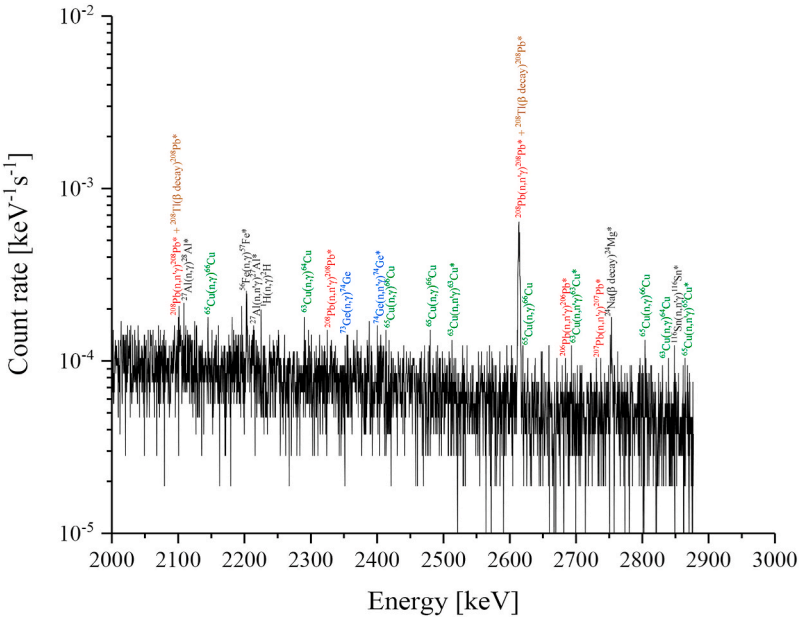

Fig. 5. Experimental HPGe detector background spectrum for energy range from 2 to 3 MeV. (Ge peaks-blue, Cu peaks-green, Pb peaks-red, contamination-brown)

origin and occurrence have been fully explained in our previous paper (Baginova et al., 2018). The triangular shape of the Ge peaks is well visible only in the energy range from 0 to 1 MeV, but not at higher energies due to poor statistics. Whereas, neutrons interact with all Ge isotopes (^{70}Ge - 20.52%, ^{72}Ge - 27.45%, ^{73}Ge - 7.76%, ^{74}Ge - 36.7% and ^{76}Ge - 7.75%) mostly by inelastic scattering, there are several Ge peaks visible in the spectra. For ^{73}Ge, there is one peak coming from this process observed at the energy of 53.44 keV. The peaks of ^{76}Ge caused by the same process are visible at the energies of 562.93 keV and 1108.41 keV. The peaks resulting from inelastic scattering of neutrons on ^{74}Ge are visible at the energies of 595.84 keV, 1204.20 keV, 1463.75 keV, 1489.35 keV, 1756.70 keV and 2402.70 keV. And finally, the ^{70}Ge peak resulting from the same reaction was found at the energy of 1039.51 keV.

The rest of the Ge peaks are caused by (n, γ) reactions, except the peak of ^{72}Ge at the energy of 691.43 keV, originating in the internal conversion. The neutron capture on ^{74}Ge nuclei led to occurrence of the ^{75}Ge peak at the energy of 139.68 keV. The ^{71}Ge peak at 708.19 keV is visible due to neutron capture on ^{70}Ge. The same process but on ^{76}Ge resulted in three peaks of ^{77}Ge at the energies of 1067.66 keV, 1353.94 keV, and 1446.87 keV. Absorption of neutrons by ^{73}Ge leads to emission of ^{74}Ge γ-line at the energy of 2353.46 keV. The Ge peaks are produced in the germanium crystal, the sensitive part of the detector.

The experimental γ-ray spectra also contain many other peaks produced by neutron interactions with materials used in the setup, especially with shielding materials. The majority belongs to copper and lead peaks, as both materials with large neutron cross sections are the most abundant in the setup.

Copper is used in the crystal holder (close to the Ge crystal), and in the copper cladding of the shield. The observed γ-lines come from inelastic scattering and capture of neutrons on copper and lead nuclei. The neutron capture prevails for copper isotopes, as it absorbs neutrons

much easier than lead thanks to larger cross sections. Gamma-lines of ^{64}Cu excited in neutron capture on ^{63}Cu were observed at the energies of 212.38 keV, 1165.21 keV, 1630.10 keV, 1670.92 keV, 1790.30 keV, 2291.42 keV and 2838.20 keV. Similarly, γ-lines of ^{66}Cu originate in neutron capture on ^{65}Cu nuclei were found at the energies of 89.18 keV, 237.82 keV, 1985.73 keV, 2144.22 keV, 2411.58 keV, 2478.20 keV, 2619.14 keV, and 2806.90 keV. The inelastic scattering led to several peaks from both copper isotopes. The ^{63}Cu peaks are visible at the energies of 955.0 keV, 962.06 keV, 1245.20 keV, 1861.30 keV, 1927.20 keV, 2512.0 keV and 2696.60 keV. The isotope ^{65}Cu gives rise to peaks at the energies of 770.60 keV, 924.50 keV, 978.80 keV, 1261.0 keV, 1832.0 keV and 2862.70 keV.

The bulk of the detector shield is made of lead, and several peaks were observed in the γ-ray spectra. The lead has four stable isotopes with relative abundance of 1.4% (^{204}Pb), 24% (^{206}Pb), 22% (^{207}Pb) and 52% (^{208}Pb). The most intensive is the 2614.51 keV line which is a superposition from the β-decay of ^{208}Tl present in the system as a radioactive impurity, and from inelastic scattering of neutrons on ^{208}Pb nuclei (as discussed in detail in the simulation chapter). Both processes, the neutron inelastic scattering and the β decay excite the same energy level of ^{208}Pb, which is the stable product of the ^{208}Tl β decay. The peaks at the energies of 2103.51 keV and 1592.51 keV are single and double escape peaks, respectively. Lead-208 lines are also visible at the energies of 583.19 keV, 860.56 keV, 1050.90 keV and 2322.65 keV. The ^{208}Pb X-rays are visible at energies of 72.81 keV and 74.97 keV. The 510.74 keV peak is supposed to be hidden in the annihilation peak. Peaks of ^{207}Pb are present in the spectra at the energies of 569.70 keV and 2736.46 keV. Lead-206 has also several γ-lines in the spectra, namely at the energies of 537.47 keV, 803.06 keV, 1620.30 keV and 2682.0 keV. Next, two lines of ^{205} Pb at the energies of 1511.0 keV and 1656.20 keV coming from neutron capture on ^{204}Pb nuclei are present in the spectra, too.

Almost all aluminium γ-rays come from the detector cryostat and the entrance window. Small amounts of aluminium are also present in the germanium crystal and in the iron absorbers as impurity. As expected, one of the main aluminium lines at the energy of 2212.01 keV is visible in the spectra. Its origin is in the third exited state of ^{27}Al and it is induced by inelastic scattering of neutrons on ^{27}Al nuclei. There is one more peak of aluminium at the energy of 2108.24 keV originating in neutron capture on ^{27}Al.

The main sources of tin peaks are in the shielding made of tin layer, and in the tin coating of the iron absorbers. The inelastic scattering was the main induction mechanism of tin γ-rays found in the spectra. Tin element has ten naturally occurring isotopes. Lines of a few of them (with the most abundant isotopes) are visible in the spectra. Tin-116 with abundance of 14.54% is identified by several lines from inelastic scattering: 1421.20 keV, 1476.75 keV, and 2850.30 keV. There is one inelastic scattering line of ^{117}Sn (abundance of 7.68%) in the spectra: 158.56 keV. There is also ^{121}Sn peak excided in neutron capture on ^{120}Sn nuclei at the energy of 966.0 keV.

All iron γ-rays are produced in the iron absorbers, resulting from inelastic scattering of neutrons on iron nuclei, and from the neutron capture. Iron has four stable isotopes, ^{54}Fe, ^{56}Fe, ^{57}Fe, and ^{58}Fe, with abundances of 5.85%, 91.75%, 2.12%, and 0.28%, respectively. The lines from inelastic scattering on ^{56}Fe are visible at 846.76 keV, 1303.4 keV and 1335.40 keV. Similarly, neutron capture excites ^{54}Fe nuclei to the energies of 1129.90 keV, 1153.10 keV. The peaks of ^{58}Fe were not observed. The peaks of ^{55}Fe and ^{57}Fe at the energies of 1917.90 keV and 2202.70 keV are an evidence of neutron capture on ^{54}Fe and ^{56}Fe, respectively. All iron γ-rays are produced in the iron absorbers.

A peak of the neutron capture on hydrogen at the energy of 2224.56 keV is seen in the third spectrum (Fig. 5.). The capture takes place on hydrogen present in plastic parts of the setup.

The peak at the energy of 477.61 keV is special. It comes from the ^{10}B (n, α)^{7}Li reaction. The outer electrode of the crystal contains boron as a semiconductor dopant and the (n, α) cross section for thermal neutrons is very high, 3838 b, so that the peak is well visible in the measured background, even if the amount of boron in the setup is very small.

The ^{24}Mg peaks at the energies of 2754.01 keV and 1368.63 keV come from the β decay of ^{24}Na produced in the ^{27}Al (n, α)^{24}Na reaction in aluminium.

We also searched for proton-induced reactions in the background spectrum. However, as the proton cosmic-ray flux at sea level is below 1% (Bogdanova et al., 2006; Povinec et al., 2008), their contributions to background should be negligible. The proton-induced peaks in (p, nγ) reactions on Ge nuclei, specifically on ^{72}Ge, ^{73}Ge, ^{74}Ge and ^{76}Ge, as well as in reactions on copper and aluminium (Baginova et al., 2018) were statistically insignificant.

The ^{64}Ni peak (1345.84 keV) witnesses EC transformation of radioactive ^{64}Cu, which was previously formed in neutron capture on ^{63}Cu, the stable isotope of copper.

The two peaks at the energies of 1173.23 keV and 1332.51 keV are de-excitation γ-rays of ^{60}Ni. They come from the β-decay of ^{60}Co produced by activation of the iron absorbers during the previous experiment involving an Am–Be neutron source (Baginova et al., 2018).

Several well visible peaks originating in natural radioactivity are present in the spectra. They come from contamination of the detector, the shield and surrounding materials, such as the laboratory walls and stuffs. Namely, ^{214}Bi resulting from β-decay of ^{214} Pb at energies of 295.22 keV and 351.93 keV and peaks of ^{214}Po coming from subsequent β-decay of ^{214}Bi detected at energies of 609.32 keV, 1120.29 keV and 1764.49 keV. Both of them belong to the ^{238}U decay chain. The peak at 2614.51 keV has double origin: β-decay of ^{208}Tl from the ^{232} Th decay series and de-excitation of ^{208}Pb excited in inelastic neutron scattering. The 1460.80 keV peak comes from the electron-capture decay of ^{40}K to de-exciting ^{40}Ar. Potassium is present as contamination from natural radionuclides in the material surrounding the detector and in the detector itself and it is also present in the iron absorbers as impurity (0.026%). Solutions of potassium-stannate and potassium-hydroxide are used as plating bath for alkali tin plating of metals (Sternfelsa and F. A. Lowenheim, 1942).

The 511 keV peak is the annihilation peak coming from annihilation of electron-positron pairs generated by photon interactions with materials of the setup.

The Compton continuum due to the material contamination is considerably lower than the cosmic-ray continuum thanks to the used low-level materials and a high detector relative efficiency. Note that no steep rise of the continuum corresponding to the Compton edge of the 2614.51 keV peak of ^{208}Tl can be observed in our experimental spectrum unlike in the experimental spectrum in (Hung et al., 2017).

5.2. Comparison of Monte Carlo simulations with the experiment

5.2.1. Simulations without the concrete building

Two simulations of the background spectrum were carried out without considering the contamination by natural radionuclides. First, a simulation without the concrete building was carried out and the resulting spectrum was compared with the measured background (Fig. 6.). There is a significant difference between the experimental and simulated spectra in the continuum below 500 keV. The main reason is that penetration of cosmic rays through the building was not in this case taken into account (the effect of the building will be discussed later). Next, contamination lines visible in the experimental spectrum and stemming from natural contamination by ^{40}K, ^{208}Tl, ^{214}Pb, and ^{214}Bi were not coded, so Compton continuum from the corresponding peaks did not contribute to count rates up to 500 keV. Several other differences were observed. The γ-ray emission for a few peaks in the energy range from 450 keV to 1 MeV is higher than in the experimental background spectrum. This effect is visible due to missing concrete shielding. Penetration via massive concrete shield reduces the γ-ray intensity in this energy range.

The triangular shape of Ge peaks coming from summation of the recoil energy in Ge nucleus and the energy of emitted γ-rays, is not simulated

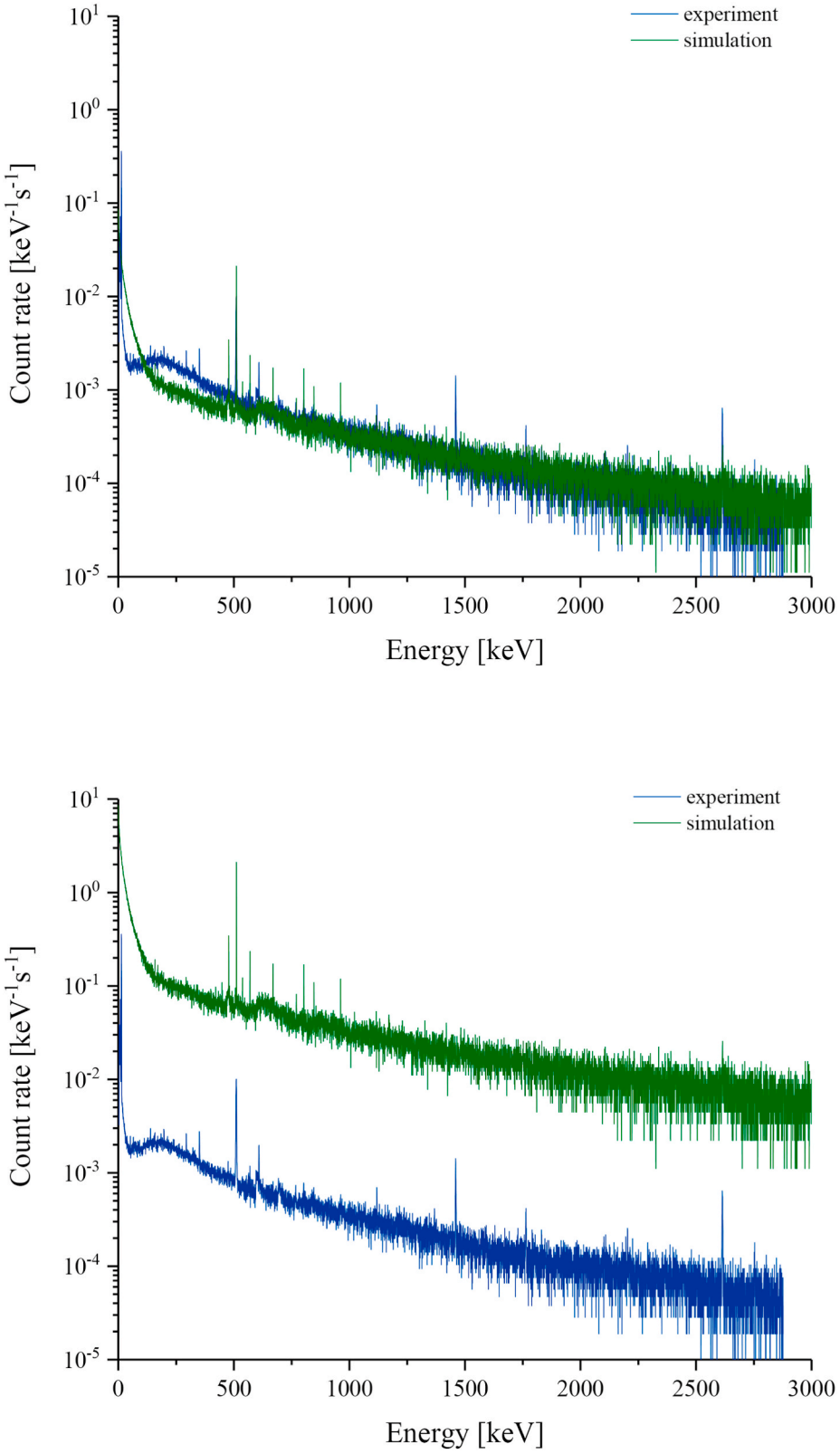

Fig. 6. Comparison of experimental and simulated HPGe background spectra (without the concrete building). The simulated spectrum shown in the bottom figure has been multiplied by 100 for better visibility.

correctly by GEANT4, as they are lower, less sharp, and their tails do not fit the real ones. The peak at the energy of 477.61 keV coming from ^{10}B (n, α)^{7}Li reaction is overestimated. The count rate of the simulated peak was approximately 5-times higher than the experimental one. The main reason is that the boron contents in the doped Ge dead layer was not known exactly. As the cross section for boron for this reaction is very high, the simulation could be affected considerably.

Special attention was paid to lead γ-rays in the simulated spectrum

(Fig. 7.). The ^{208}Pb peaks known as originating in β-decay of ^{208}Tl, usually present in detector systems as a contaminant, are clearly visible also in the simulated spectrum, although no contamination was assumed. The γ-lines come from the inelastic scattering of neutrons on ^{208}Pb nuclei. The count rates of the main ^{208}Pb peak (2614.51 keV) were compared. It is 0.00048 ± 0.00014 s^{-1} for the experimental peak and 0.00024 ± 0.00007 s^{-1} for the simulated one. The count rate is higher in the measured than in the simulated background, indicating that there is also a direct contribution from ^{208}Tl decay, as expected. It can be concluded that, approximately 50% of the peak in the measured background spectrum is formed by neutron interactions with ^{208}Pb nuclei. Therefore, as long as lead will be present in the experimental setup, these peaks will be present in the background spectrum, even if the contamination with ^{208}Tl would be eliminated.

The experimental and the simulated spectra were compared by integral count rates for the energy range from 500 keV to 2875 keV where the spectra match each other. The integral count rate measured in the experiment 0.56 ± 0.03 s^{-1} was in a very good agreement with the calculated value 0.53 ± 0.05 s^{-1}. However, omission of the roof shielding in the simulation results in a considerable difference between the measured and simulated spectra below 500 keV. The roof shielding is apparently a very important part of the simulation setup as will be shown in the next Section.

5.2.2. *Simulations including the concrete building*

Another simulation of background γ-ray spectrum was carried out, this time taking the building into account. The shape of the simulated spectrum replicates the experimental one much better than when the building effect was omitted (Fig. 8.). This time, the typical wide hump in the continuum around 200 keV is predicted well. However, there is still a slight difference in the continuum heights up to 350 keV, probably caused by omission of radionuclide contamination of construction materials in the simulations. The simulated continuum is slightly lower, especially in the part below the ^{214}Bi peaks. The simulated peak of ^{7}Li at the energy of 477.61 keV is again overestimated, but the count rate of the simulated peak decreased by about a factor of two. The count rates of the ^{208}Pb peaks at the energy of 2614.51 keV were compared again. The experimental one is 0.00048 ± 0.00014 s^{-1}, while the simulated one is 0.00017 ± 0.00005 s^{-1}, what means that approximately 35% of the experimental peak originate in inelastic scattering of neutrons on lead nuclei. The count rate of the simulated peak is lower than in the previous simulation (without the concrete) by 30%, what can be explained by changed neutron spectral fluxes after passing the concrete layer. Due to same reason, the triangular shape of Ge peaks is less visible as it was in the simulation without the concrete layer.

Integral count rates of the experimental and simulated spectra were compared for the energy region from 50 to 2875 keV taking into account the concrete shielding. Below the energy of 50 keV, the count rate is strongly influenced even by small changes in the thicknesses and material composition of various layers. Therefore, it is difficult to achieve quantitative agreement of count rates below this energy. Integral count rate of the measured spectrum 1.26 ± 0.07 s^{-1} matches the simulated one of 1.25 ± 0.13 s^{-1}, indicating a very satisfactory agreement. The numerical difference of less than 1% is rather a random coincidence than a precise result match. It may seem that, in the region above 2000 keV, the simulated count rate is higher than the measured one (Fig. 8.). Therefore, the integral count rates (continuum and peaks) were calculated for both spectra in the energy range from 2000 keV to the end of the measured spectrum at 2875 keV. The obtained count rates were 0.07 ± 0.005 s^{-1} for the experimental spectrum and 0.08 ± 0.009 s^{-1} for the simulated one (only statistical uncertainties at the 1σ level). The experimental spectrum shows greater statistical fluctuations, which are more pronounced at lower values in the logarithmic *y* scale.

The measured and simulated results are listed in Table 1 accompanying this paper. The count rates of measured and simulated peaks were compared (Fig. 9.) and it was found that the simulated peaks fit the experimental ones very reasonably. There are only two outliers that cannot be explained by statistical uncertainties visible in the plot, ^{7}Li (477.61 keV) and ^{208}Pb (2614.51 keV) peaks discussed above. The simulated annihilation peak fits the measured one very well. Very high uncertainties of the rest of the peaks, did not allow us to make their rigorous quantitative comparison. There is tendency to underestimate the simulated peak count rates, what is understandable due to complexity of interactions leading to induction of these peaks. Certain processes cannot be simulated by GEANT4 at all.

No information about radionuclide contamination of different parts of the setup was available, therefore, no rigorous simulation of the background spectrum due to the contamination was possible. Moreover, a large part of the measured count rates (with the exception of ^{40}K), may be caused by presence of radon (^{222}Rn) and thoron (^{220}Rn) in the detector construction and shielding materials, and their decay close to the Ge detector (Vojtyla, 1995), as the laboratory did not have a ventilation

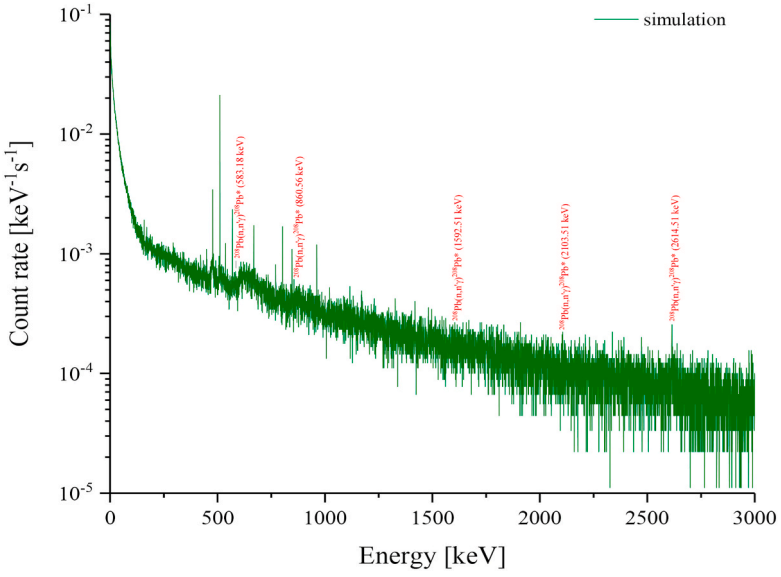

Fig. 7. Simulation with those γ-rays of ^{208}Pb coming from inelastic scattering of neutrons on lead nuclei, which correspond to γ-rays of ^{208}Tl decay if thallium is present in the setup.

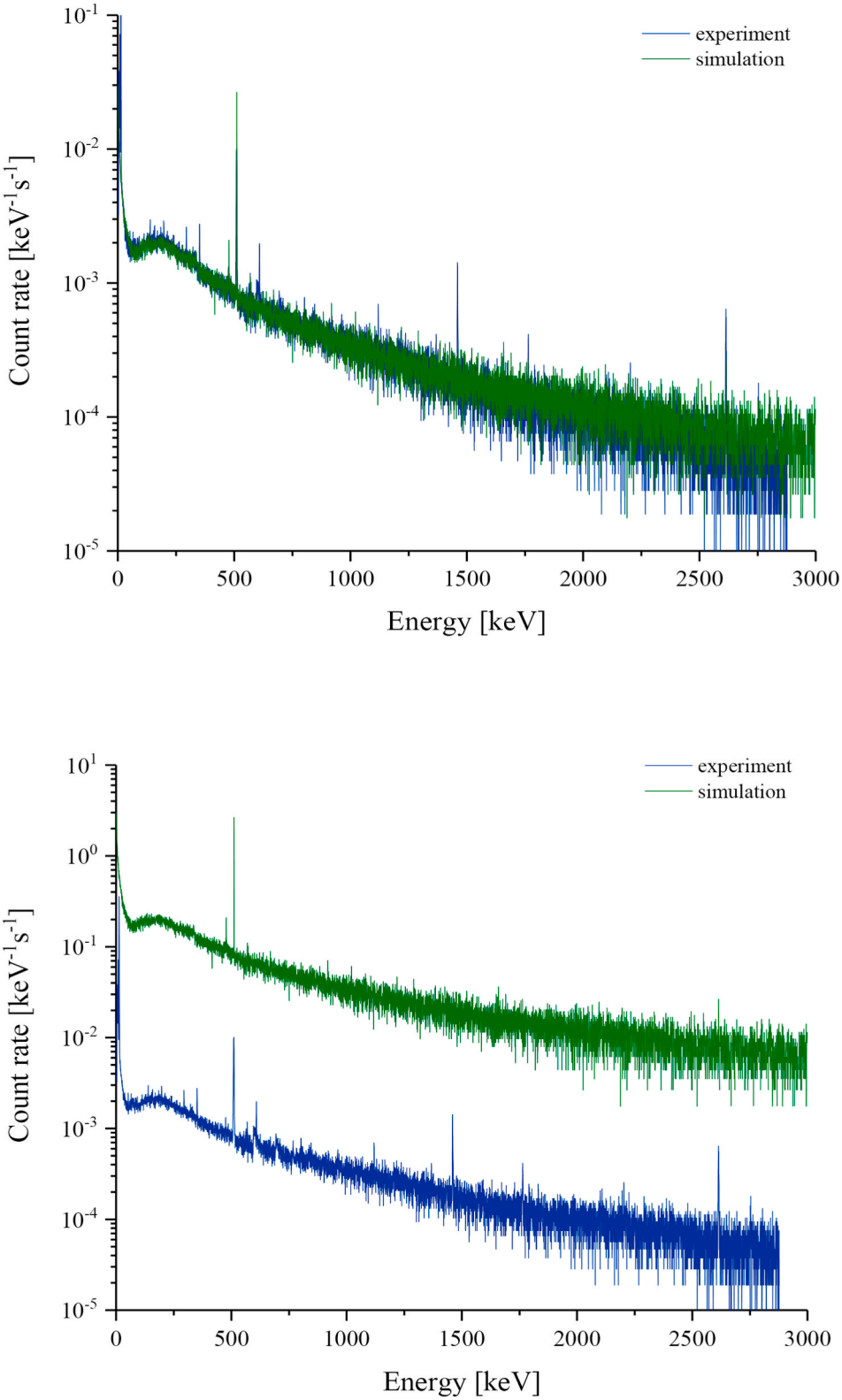

Fig. 8. Comparison of the experimental spectrum and the simulated spectrum when the concrete building was included in the setup. The simulated spectrum shown in the bottom figure has been multiplied by 100 for better visibility.

Table 1
Calculated count rates in measured background γ-ray spectrum and simulated ones with and without the shielding layer of the building (uncertainties are quoted at 1σ).

Energy peaks [keV]	Nuclides and Reactions	Count rates × 10^{-5} [s^{-1}]		
		Experiment	Simulation (without concrete building)	Simulation (with concrete building)
50–2875	Continuum	(1.26 ± 0.07) × 10^5		(1.25 ± 0.13) × 10^5
500–2875	Continuum	(0.56 ± 0.03) × 10^5	(0.53 ± 0.06) × 10^5	
53.44	^{73}Ge (n, n'γ)^{73}Ge*	30 ± 13	32 ± 25	26 ± 13
72.81	X-rays of ^{208}Pb	10 ± 6	12 ± 9	12 ± 6
74.97	X-rays of ^{208}Pb	27 ± 13	13 ± 9	20 ± 12
89.18	^{65}Cu(n, γ)^{66}Cu*	10 ± 6	18 ± 8	10 ± 6
139.68	^{74}Ge (n, γ)^{75}Ge*	31 ± 14	22 ± 13	27 ± 13
158.56	^{117}Sn(n, n'γ)^{117}Sn*	14 ± 7	21 ± 12	9 ± 6
212.38	^{63}Cu(n, γ)^{64}Cu*	35 ± 13	21 ± 16	30 ± 13
237.82	^{65}Cu(n, γ)^{66}Cu*	39 ± 13	20 ± 10	38 ± 19
295.22	^{214}Pb(β decay)^{214}Bi*	101 ± 20	–	–
351.93	^{214}Pb(β decay)^{214}Bi*	146 ± 19	–	–
477.61	^{10}B (n, α)^{7}Li	22 ± 8	120 ± 12	51 ± 10
511.0	Annihilation	814 ± 46	757 ± 49	943 ± 69
537.47	^{206}Pb(n, n'γ)^{206}Pb*	15 ± 10	23 ± 9	17 ± 4
562.93	^{76}Ge (n, n'γ)^{76}Ge*	8 ± 4	4 ± 3	13 ± 7
569.70	^{207}Pb(n, n'γ)^{207}Pb*	21 ± 9	42 ± 6	15 ± 4
583.19	^{208}Pb(n, n'γ)^{208}Pb*	12 ± 8	7 ± 4	5 ± 3
595.84	^{74}Ge (n, n'γ)^{74}Ge*	33 ± 13	18 ± 11	21 ± 11
609.32	^{214}Bi(β decay)^{214}Po*	206 ± 23	–	–
691.43	^{72}Ge (n, n'e)^{72}Ge*	28 ± 11	12 ± 8	11 ± 7
708.19	^{70}Ge (n, γ)^{71}Ge*	14 ± 7	10 ± 8	6 ± 3
770.60	^{65}Cu(n, n'γ)^{65}Cu*	11 ± 7	10 ± 4	13 ± 7
803.06	^{206}Pb(n, n'γ)^{206}Pb*	29 ± 11	36 ± 6	24 ± 10
846.76	^{56}Fe (n, n'γ)^{56}Fe*	17 ± 7	9 ± 3	8 ± 3
860.56	^{208}Pb(n, n'γ)^{208}Pb*	10 ± 6	5 ± 3	7 ± 3
924.50	^{65}Cu(n, n'γ)^{65}Cu*	7 ± 3	5 ± 3	6 ± 5
955.0	^{63}Cu(n, n'γ)^{63}Cu*	6 ± 3	11 ± 6	5 ± 3
962.06	^{63}Cu(n, n'γ)^{63}Cu*	12 ± 7	28 ± 5	15 ± 6
966.0	^{120}Sn(n, γ)^{121}Sn*	10 ± 5	8 ± 3	5 ± 3
978.80	^{65}Cu(n, n'γ)^{65}Cu*	8 ± 3	6 ± 3	4 ± 2
1039.51	^{70}Ge (n, n'γ)^{70}Ge*	13 ± 5	13 ± 8	6 ± 3
1050.90	^{208}Pb(n, n'γ)^{208}Pb*	6 ± 3	4 ± 2	6 ± 3
1067.66	^{76}Ge (n, γ)^{77}Ge*	9 ± 5	6 ± 3	5 ± 3
1108.41	^{76}Ge (n, n'γ)^{76}Ge*	21 ± 5	11 ± 6	10 ± 5
1120.29	^{214}Bi(β decay)^{214}Po*	17 ± 7	–	–
1129.90	^{54}Fe (n, n'γ)^{54}Fe*	16 ± 8	11 ± 6	10 ± 5
1153.10	^{54}Fe (n, n'γ)^{54}Fe*	6 ± 3	4 ± 2	7 ± 5
1165.21	^{63}Cu(n, γ)^{64}Cu*	14 ± 5	10 ± 5	11 ± 5
1173.23	^{60}Co(β decay)^{60}Ni*	9 ± 5	–	–
1204.20	^{74}Ge (n, n'γ)^{74}Ge*	10 ± 5	8 ± 5	4 ± 2
1245.20	^{63}Cu(n, n'γ)^{63}Cu*	4 ± 2	3 ± 2	4 ± 2
1261.0	^{65}Cu(n, n'γ)^{65}Cu*	13 ± 7	10 ± 5	10 ± 4
1303.40	^{56}Fe (n, n'γ)^{56}Fe*	18 ± 6	10 ± 5	10 ± 4
1332.51	^{60}Co(β decay)^{60}Ni*	14 ± 6	–	–
1335.40	^{56}Fe (n, n'γ)^{56}Fe*	14 ± 4	8 ± 5	7 ± 4
1345.84	^{64}Cu(ε decay)^{64}Ni*	16 ± 7	7 ± 4	6 ± 2
1353.94	^{76}Ge (n, γ)^{77}Ge*	11 ± 4	8 ± 5	5 ± 2
1368.63	^{24}Na (β decay)^{24}Mg*	13 ± 8	7 ± 5	6 ± 4
1421.20	^{116}Sn(n, n'γ)^{116}Sn*	10 ± 4	6 ± 4	6 ± 2
1446.87	^{76}Ge (n, γ)^{77}Ge*	7 ± 4	6 ± 4	6 ± 4
1460.80	^{40}K (β decay)^{40}Ar*	115 ± 16	–	–
1463.75	^{74}Ge (n, n'γ)^{74}Ge*	5 ± 2	9 ± 4	10 ± 4
1476.75	^{116}Sn(n, n'γ)^{116}Sn*	13 ± 4	6 ± 4	10 ± 4
1489.35	^{74}Ge (n, n'γ)^{74}Ge*	11 ± 4	5 ± 4	5 ± 2
1511.0	^{204}Pb(n, γ)^{205}Pb*	9 ± 4	4 ± 2	4 ± 2
1592.51	Single escape peak of 2614.51 keV	12 ± 6	14 ± 7	7 ± 4
1620.30	^{206}Pb(n, n'γ)^{206}Pb*	6 ± 4	7 ± 4	7 ± 4
1630.10	^{63}Cu(n, γ)^{64}Cu*	6 ± 4	8 ± 5	4 ± 2
1656.20	^{204}Pb(n, γ)^{205}Pb*	5 ± 3	6 ± 4	10 ± 4
1756.70	^{74}Ge (n, n'γ)^{74}Ge*	7 ± 3	9 ± 4	5 ± 2
1764.49	^{214}Bi(β decay)^{214}Po*	26 ± 9	–	–
1790.30	^{63}Cu(n, γ)^{64}Cu*	5 ± 2	4 ± 2	3 ± 3
1832.0	^{65}Cu(n, n'γ)^{65}Cu*	9 ± 5	9 ± 6	5 ± 3
1861.30	^{63}Cu(n, n'γ)^{63}Cu*	8 ± 3	10 ± 3	5 ± 3
1917.90	^{54}Fe (n, γ)^{55}Fe*	6 ± 3	8 ± 4	8 ± 3
1927.20	^{63}Cu(n, n'γ)^{63}Cu*	8 ± 3	10 ± 4	7 ± 3
1985.73	^{65}Cu(n, γ)^{66}Cu*	5 ± 2	6 ± 2	4 ± 2
2103.51	Double escape peak of 2614.51 keV	8 ± 3	10 ± 4	6 ± 3
2108.24	^{27}Al (n, γ)^{28}Al*	4 ± 2	5 ± 2	7 ± 3
2144.22	^{65}Cu(n, γ)^{66}Cu*	6 ± 3	7 ± 4	4 ± 2
2202.70	^{56}Fe (n, γ)^{57}Fe*	4 ± 2	5 ± 2	4 ± 2

(*continued on next page*)

Table 1 (*continued*)

Energy peaks [keV]	Nuclides and Reactions	Count rates × 10^{-5} [s^{-1}]		
		Experiment	Simulation (without concrete building)	Simulation (with concrete building)
2212.01	^{27}Al (n, n'γ)^{27}Al*	6 ± 3	8 ± 4	4 ± 1
2224.56	^{1}H (n, γ)^{2}H	6 ± 3	7 ± 3	6 ± 3
2291.42	^{63}Cu(n, γ)^{64}Cu*	8 ± 3	4 ± 2	8 ± 4
2322.65	^{208}Pb(n, n'γ)^{208}Pb*	6 ± 2	8 ± 3	4 ± 3
2353.46	^{73}Ge (n, γ)^{74}Ge*	5 ± 3	7 ± 3	4 ± 3
2402.70	^{74}Ge (n, n'γ)^{74}Ge*	5 ± 2	6 ± 3	5 ± 4
2411.58	^{65}Cu(n, γ)^{66}Cu*	4 ± 1	4 ± 2	5 ± 3
2478.20	^{65}Cu(n, γ)^{66}Cu*	4 ± 1	4 ± 2	4 ± 3
2512.0	^{63}Cu(n, n'γ)^{63}Cu*	4 ± 2	5 ± 3	4 ± 2
2614.51	^{208}Pb(n, n'γ)^{208}Pb*	48 ± 14	24 ± 7	17 ± 4
2619.14	^{65}Cu(n, γ)^{66}Cu*	4 ± 2	5 ± 3	5 ± 3
2682.0	^{206}Pb(n, n'γ)^{206}Pb*	4 ± 2	5 ± 3	2 ± 1
2696.60	^{63}Cu(n, n'γ)^{63}Cu*	4 ± 2	5 ± 3	4 ± 2
2736.46	^{207}Pb(n, n'γ)^{207}Pb*	5 ± 2	3 ± 1	3 ± 2
2754.01	^{24}Na (β decay)^{24}Mg*	4 ± 3	4 ± 3	3 ± 1
2806.90	^{65}Cu(n, γ)^{66}Cu*	5 ± 2	7 ± 3	3 ± 1
2838.20	^{63}Cu(n, γ)^{64}Cu*	4 ± 2	5 ± 3	8 ± 3
2850.30	^{116}Sn(n, n'γ)^{116}Sn*	4 ± 1	4 ± 1	4 ± 2
2862.70	^{65}Cu(n, n'γ)^{65}Cu*	3 ± 1	4 ± 1	4 ± 2

system removing these inert gases and their progeny from the ambient air. The average activities of radon and thoron in the shield may vary with time and their reliable quantification is difficult. Investigation of the effect of material contamination may be a subject of further studies if the material contamination will be known. Other background sources than radioactive contamination dominate the background continuum in systems of this class located in surface laboratory.

The continuum in HPGe background spectrum is formed mainly by muon and neutron interactions. Neutrons interacting with the detector materials, especially with lead, produce many photons contributing to the continuum, while muons contribute via bremsstrahlung of delta electrons. A continuum is, however, not induced only by cosmic ray particles. Part of it is formed by radioactive contaminants present in the system. Further contributors are, therefore, β-rays originating from decaying radionuclides and Compton scattering coming from interactions of high-energy photons (Povinec, 2007). In particular, commercial lead used for shielding of HPGe detectors is contaminated with ^{210}Pb. In surface laboratories this background component is not distinguishable from the low-energy part of continuum induced mainly by muons (Vojtyla, 1996a).

To estimate the contribution of radioactive contamination to the detector continuum, a number of simulations with ^{238}U, ^{232}Th, and ^{40}K in the setup materials, and ^{222}Rn in air inside the shield cavity were run. The resulting simulation spectra were normalized so that the simulated and the experimental count rates of the contamination peaks agreed while assuming that 35% of the ^{208}Tl peak at 2614.5 keV was induced by

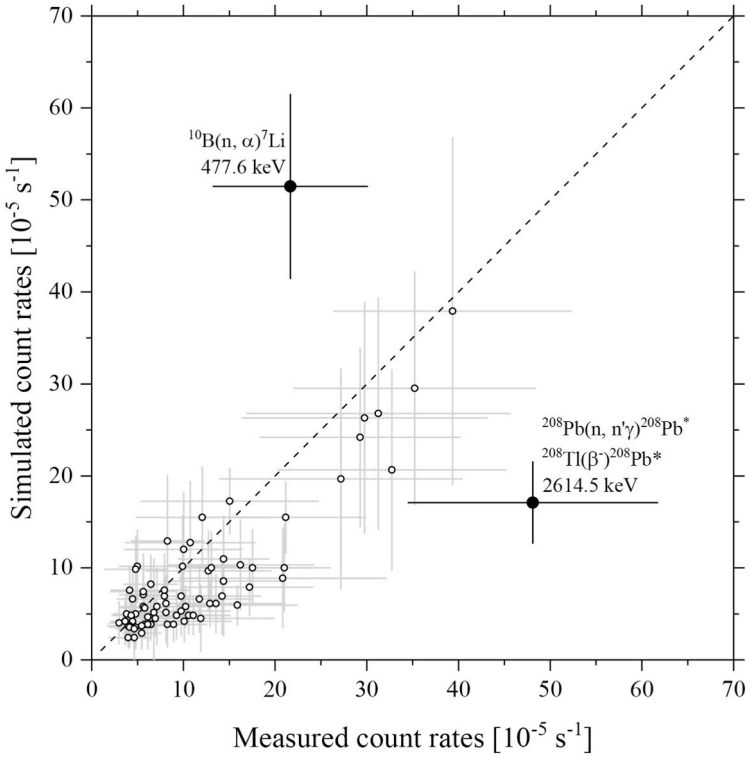

Fig. 9. Comparison of the experimental and simulated peak count rates.

neutrons. It was found that the simulated integral count rate 0.033 ± 0.006 s^{-1} (50–2875 keV) due to radioactive contamination of the simulated spectrum made 2.6% of the total experimental integral count rate 1.26 ± 0.07 s^{-1}. This figure perfectly agrees with the fraction of integral count rate of 2.4% obtained by subtracting the simulated spectrum from the experimental one. Indeed, continua observed in the experimental spectra of low-level HPGe spectrometers operating in surface or shallow laboratories are mostly induced by cosmic rays.

5.2.3. Comparison of the simulated results with published works

Although the GEANT4 code has been originally developed for high energy physics, after many applications in low energy nuclear physics it has proved to be a well-suited code for estimation of neutron fluxes and their interactions with nuclei in surface as well as in underground laboratories (Baginova et al., 2018; Kudryavtsev et al., 2008). The second important input in the simulations is the neutron transport in matter. GEANT4 has been successfully used for neutron tracking in the energy range of interest and in the materials, which were used in the present investigations. The GEANT4 ability to model neutron propagation through matter has been confirmed with cosmic-ray neutrons as well with neutrons from neutron sources (e.g., Ljungvall and Nyberg, 2005; Baginova et al., 2018).

Successful simulations of neutron-induced reactions we need to use accurate correct neutron cross-section data. We already discussed in detail neutron cross-sections we used in this work, and on the basis of our previous experiences (Kudryavtsev et al., 2008; Baginova et al., 2018) we may confirm that the most recent cross-sections were used in the presented calculations.

However, the best way how to validate the model is to compare the simulation products with the experiment, as well as with similar already published results. The simulated results are reliable and they agree with the experimental data (Figs. 8., 9.), as well as with published data.

Several papers have already been dealing with Monte Carlo simulations of background of HPGe detectors operating in surface or shallow underground laboratories (e.g. Vojtyla, 1995, 1996b; Povinec et al., 2008; Breier and Povinec, 2009; Hung et al., 2017).

From the experimental point of view, the γ-lines identified in the experimental background spectrum, which are due to neutron interactions with HPGe detector materials were also seen in previous investigations of neutron-induced γ-ray spectra (Chao, 1993; Vojtyla et al., 1994, Ljungvall and Nyberg, 2005; Jovancevic et al., 2010; Baginova et al., 2018).

The shape of the background γ-ray spectrum was dominated by muon-induced hump with the maximum at energy of 185 keV, similarly as it was observed in previous investigations (Vojtyla et al., 1994, Vojtyla, 1995; Breier and Povinec, 2009; Hung et al., 2017). This background γ-ray spectrum feature is well visible in the experimental (Fig. 3.) as well as in the simulated spectra (Fig. 8.), in agreement with previous measurements and Monte Carlo simulations in the above mentioned works. In (Hung et al., 2017) a SEGe detector with a relative efficiency of 20% was used in an experiment and coded into GEANT4 simulation. The simulated count rate on the top of the hump was about 7.6×10^{-4} $keV^{-1}s^{-1}$. After normalization of our value of 2.2×10^{-4} $keV^{-1}s^{-1}$ to a 20% detector, one obtains 8.8×10^{-4} $keV^{-1}s^{-1}$ indicating a good agreement. In the higher energy part of the continuum at 2000 keV (Hung et al., 2017), got 4.0×10^{-5} $keV^{-1}s^{-1}$ to be compared with the value from this work of $1.1 \times 10^{-}$ $keV^{-1}s^{-1}$. Scaling this value to a 20% detector leads to a spectral count rate of 4.4×10^{-5} $keV^{-1}s^{-1}$, which is consistent with the figure from (Hung et al., 2017).

The count rate on the top of the hump in (Vojtyla, 1995) calculated with a 35% HPGe detector is about 1.6×10^{-3} $keV^{-1}s^{-1}$ (Fig. 6 in the reference). After normalization to 50% relative efficiency, one obtains 1.5×10^{-3} $keV^{-1}s^{-1}$.

In the work (Breier and Povinec, 2009), the cosmic-ray background of an HPGe detector with a relative efficiency of 70% in various shields placed on the surface and 10 m. w.e. underground was simulated. The count rate at the maximum of the 200 keV hump shown in Fig. 5 in reference (10 cm lead shield) is about 1.6×10^{-3} s^{-1}. After normalization of our hump count rate to the 70% efficiency one gets 3.1×10^{-3} $keV^{-1}s^{-1}$.

Table 2
Comparison of simulated cosmic-ray spectra from the literature.

Size	Reference	(1)	(2)	(3)	(4)
		keV^{-1} s^{-1}			
20%	Hung et al. (2017)	7.2×10^{-4}	8.8×10^{-4}	4.0×10^{-5}	4.4×10^{-5}
35%	P. Vojtyla et al., 1995	1.6×10^{-3}	1.5×10^{-3}	–	–
50%	This work	2.2×10^{-3}	2.2×10^{-3}	1.1×10^{-4}	1.1×10^{-4}
70%	Breier and Povinec, 2009	1.6×10^{-3}	3.1×10^{-3}	–	–

[1] Spectral count rate on the top of the hump as obtained from the Reference.
[2] Spectral count rate on the top of the hump from this work normalized to the given relative efficiency.
[3] Spectral count rate at 2 MeV as obtained from the Reference.
[4] Spectral count rate at 2 MeV from this work normalized to the given relative efficiency.

Values obtained from different sources are summarized in Table 2. The results in this work agree fairly well with the data from the literature if they are normalized to the relative efficiency of the given detector, except the work (Breier and Povinec, 2009). The simulated shield was made only of lead, while the other simulated shields were lined from the inner side with descending-*Z* layers (e.g. Sn and Cu, Cd and Cu) (Vojtyla, 1996b). showed that the height of the spectrum hump depended strongly on *Z* of the innermost shield material – the heavier the material was – the lower was the hump maximum count rate. In the extreme case of a purely lead shield and a purely copper shield, the latter shield provided a count rate 4.5 higher compared with the one of the former shield. The difference in the lining material could explain the lower values reported in (Breier and Povinec, 2009).

The annihilation peak dominated in all experimental and simulated spectra of the above mentioned studies. Nevertheless, the triangular germanium peaks are observable only in our and (Vojtyla et al., 1995) measured background spectra. The visibility of such peaks is highly affected by relative efficiency and resolution of the used HPGe detector, and by a sufficiently long measuring time. In simulated spectra these peaks are not well visible, because GEANT4 is not yet capable to simulate correctly the processes leading to these peaks. The integral count rate of the background simulated in this work of 1.25 ± 0.13 s^{-1} is within the range of 0.6–1.6 s^{-1} stated in (Povinec, 2012).

6. Material optimization

In addition to passive cosmic-ray flux reduction and anti-coincidence pulse-rejection techniques, material selection with regard to nuclear interactions is a way of lowering the cosmic-ray induced background.

Besides germanium, copper and lead are the most significant contributors to the neutron background. Copper and lead peaks evidently dominate in all three spectra. All γ-lines produced in neutron interactions with these materials form together a strong source of the neutron background. This source of background is specifically disturbing, because it covers large part of the energy range of HPGe detector and like this, it can easily hide or imitate the searched signal. To find the real signal is extremely important for experiments looking for rare events. For example, the γ-rays coming from neutron inelastic scattering or neutron capture can imitate the signature of the neutrinoless ββ decay (Kudryavtsev et al., 2008). In addition, some of the ^{208}Pb peaks are enhanced by the γ-rays from β-decay of ^{208}Tl. The best way how to avoid such large amount of neutron induced peaks from lead and copper is to replace them by other types of materials or at least combine them with

neutron reducing materials.

Similarly, γ-lines of tin contribute to neutron background. Neutrons interacting with tin parts of the setup, especially with the tin layer of the shield produce many γ-rays. Avoid this contributor is possible by omitting the tin from the setup, especially from the shielding. Shields in deep underground experiments are made mostly of pure lead, so there is no tin present.

Aluminium and iron have a few γ-lines in the background spectrum produced by neutron interactions. They are certainly less significant background components than lead or copper but they contribute to neutron background, too. Aluminium is the most commonly used material for cryostats, entrance windows and sometimes also for crystal holders. Thus, the aluminium peaks will be permanently present in the background spectrum, but reduction of neutron flux can help to minimize them. Iron is usually minimally used as material in the detector setup. There is certain amount of iron in the cooling tube delivering the liquid nitrogen to the detector, but its influence can be eliminated by suitable placing of the shied around the detector, which will shield the tube. Simply, forego the iron peaks is possible by excluding the iron materials from the setup.

The peaks of natural radionuclides coming from contamination of the detector parts, the shield and surrounding form together the γ-ray induced background. To eliminate these peaks is difficult because the radionuclides are present everywhere and they are permanently produced by decay of members of uranium and thorium series. To minimize the influence of γ-rays from natural radionuclides, it is necessary to use ultra-high purity materials for experimental setups and to predict the amount of the contaminants and their activity. The reduction of such peaks is possible using an appropriate shielding, too. Anyway, even in deep underground laboratories is contamination still present.

7. Conclusions

The presented work deals with experimental and theoretical (GEANT4) investigations of background induction mechanisms of a low-level 50% p-type HPGe gamma spectrometer placed in a descending-Z lead shield (Pb–Sn–Cu). The whole system is located on the surface, on the ground floor of a 3-storey building providing around 1 m of concrete bulk shielding. Particular attention is given to clarifying the role of secondary and tertiary cosmic-ray neutrons.

A very good agreement, qualitative as well as quantitative, between the measured and simulated spectra was achieved, confirming that GEANT4 is a suitable detector simulation tool for this type of studies, even if very complex neutron interactions with matter are involved. Nevertheless, triangular peaks, which are characteristic of neutron interactions with Ge crystals, cannot be reproduced correctly at present. The shapes of these peaks reflect particularities of the detection mechanism such as the recoil dynamics and plasma effects in charge collection.

The background continuum in an HPGe system of this class (low-level in a surface building with moderate overhead shielding) is generated mostly by cosmic-ray muons and tertiary cosmic-ray neutrons. The latter are responsible for almost all γ-ray lines of cosmic-ray origin in the background spectrum. The main sources of neutron-induced γ-rays are, except the Ge crystal, lead, copper and tin present in the construction materials of the HPGe detector and in the shield. An extensive list of γ-lines potentially visible in a background spectrum was compiled and the main nuclear reactions generating them were identified. It was found, that the source of the well-known 2614.51 keV peak is not exclusively the β-decay of ^{208}Tl from the ^{232}Th decay series to an excited state of the stable daughter nuclide ^{208}Pb. The inelastic neutron scattering on ^{208}Pb nuclei abundantly present in the lead shield contributes by about 35% to this peak.

Below about 500 keV, the shape of the background continuum predominantly generated by cosmic rays (mainly by muons and neutrons) in our case depends considerably on the thickness of the overhead concrete bulk shielding associated with the building in which the system is located. Generally, there has been reasonable agreement between the measured and simulated background γ-ray spectra. The final integral counting rates for measured spectrum in the energy range from 50 keV to 2875 keV was $1.26 \pm 0.07\ s^{-1}$ and for simulated one $1.25 \pm 0.13\ s^{-1}$, indicating very good agreement with the experiment.

Peaks caused by radioactive contamination of the system were detected and traced to the primordial ^{40}K and a few members of the ^{238}U and ^{232}Th decay series (^{214}Bi, ^{214}Pb, ^{208}Tl). Yet, in the case of the present system, the lack of knowledge of construction material contamination and probable interference of radon and thoron entering the shield cavity did not allow us to investigate this background source theoretically. The issue can be a subject of further studies for detector systems with known contamination placed in rooms with radon and thoron free air.

Although Pb and Cu are very popular materials for construction of low-level HPGe detector systems thanks to their costs and achievable purity, they are not the ideal choice as far as the neutron background is concerned. Interaction cross-sections are large and too many γ-rays are produced in nuclear reactions of various types. Tin should be also avoided as a construction material.

Apparently, no ideal solution is available when dealing with construction materials, however, deeper knowledge of the topic and the tools used in this work are useful in the search for an optimum.

CRediT authorship contribution statement

M. Baginova: Conceptualization, Methodology, Software, Formal analysis, Investigation, Data curation, Writing - original draft. **P. Vojtyla:** Resources, Writing - review & editing. **P.P. Povinec:** Supervision, Writing - review & editing.

Declaration of competing interest

The authors declare that they have no known competing financial interests or personal relationships that could have appeared to influence the work reported in this paper.

Acknowledgments

The authors are thankful to CERN for providing PhD fellowship to Miloslava Baginova. Special thanks to Fabrice Malacrida for his help with the experiment. Support provided by the Slovak Research and Development Agency (APVV-15-0576) is highly acknowledged.

References

Abdelhameed, A.H., et al., 2019. Geant4-based electromagnetic background model for the CRESST dark matter experiment. Eur. Phys. J. C 79, 881.
Adhikari, G., et al., 2018. Initial performance of the COSINE-100 experiment. Eur. Phys. J. C 78, 107.
Agostinelli, S., et al., 2003. Geant4 – a simulation toolkit. Nucl. Instrum. Methods Phys. Res. 506, 250–303.
Allison, J., et al., 2006. Geant4 developments and applications. IEEE Trans. Nucl. Sci. 53, 270–278.
Allison, J., et al., 2016. Recent developments in Geant4. Nucl. Instrum. Methods Phys. Res. 835, 186–225.
Armengaud, E., et al., 2017. Performance of the EDELWEISS-III experiment for direct dark matter searches. J. Inst. Met. 12, P08010.
Baginova, M., Vojtyla, P., Povinec, P.P., 2018. Investigation of neutron interactions with Ge detectors. Nucl. Instrum. Methods Phys. Res. 897, 22–31.
Bogdanova, L.N., et al., 2006. Cosmic muon flux at shallow depth underground. Phys. Atom. Nucl. 69, 1328–1333.
Breier, R., Povinec, P.P., 2009. Monte Carlo simulation of background characteristics of low-level gamma-spectrometers. J. Radioanal. Nucl. Chem. 799–804.
Chao, J.H., 1993. Neutron-induced gamma-rays in germanium detectors. Appl. Radiat. Isot. 44, 605–611.
Geant4 Collaboration. Introduction to Geant4. available at. http://geant.cern.ch/ (accessed on June 19th, 2019).
Greider, P.K.F., 2001. Cosmic Rays at Earth. Researcher's Reference and Data Book Manual, first ed. Elsevier, Amsterdam.
Hung, N.Q., et al., 2017. Investigation of cosmic-ray induced background of Germanium gamma spectrometer using GEANT4 simulation. Appl. Radiat. Isot. 121, 87–90.

Jovancevic, N., et al., 2010. Neutron induced background gamma activity in low-level Ge-spectroscopy systems. Nucl. Instrum. Methods Phys. Res. 612, 303–308.
Kauer, M., The SuperNEMO Collaboration 2008, 2009. Calorimeter R&D for the SuperNEMO double beta decay experiment. J. Phys.: Conf. Ser. 160, 012031.
Kudryavtsev, V.A., et al., 2008. Neutron- and muon-induced background in underground physics experiments. Europ. Phys. J. A 36, 171–180.
Ljungvall, J., Nyberg, J., 2005. A study of fast neutron interactions in high-purity germanium detectors. Nucl. Instrum. Methods Phys. Res. 546, 553–573.
Medhat, M.E., Wang, Y., 2014. Estimation of background spectrum in a shielded HPGe detector using Monte Carlo simulations. Appl. Radiat. Isot. 84, 13–18.
Nuclear Data Center. Japan atomic energy agency (JAEA). available at: http://wwwndc.jaea.go.jp/jendl/j40/j40.html (accessed on June 19th, 2019).
Povinec, P.P., 2007. Analysis of Environmental Radionuclides, first ed. Elsevier, Oxford.
Povinec, P.P., et al., 2008. New isotope technologies in environmental physic. Acta Phys. Slovaca 58 (1), 1−154.
Povinec, P.P., 2012. New gamma-spectrometry technologies for environmental sciences. J. Analyt. Sci. Tech. 42–71.
Shun-Li, N., et al., 2015. Simulation of background reduction and Compton suppression in a low-background HPGe spectrometer at a surface laboratory. Chin. Phys. C 39, 086002.
Sternfelsa, M.M., Lowenheim, F.A., 1942. Tin plating from the potassium stannate bath. J. Electrochem. Soc. 82, 77–100.
Vojtyla, P., et al., 1994. Experimental and simulated cosmic muon induced background of a Ge spectrometer equipped with a top side anticoincidence proportional chamber. Nucl. Instrum. Methods Phys. Res. B 86, 380–386.
Vojtyla, P., 1995. A computer simulation of the cosmic-muon background induction in a Ge γ-spectrometer using GEANT. Nucl. Instrum. Methods Phys. Res. B 100, 87–96.
Vojtyla, P., 1996a. Fast computer simulations of background of low-level Ge γ-spectrometers induced by ^{210}Pb/^{210}Bi in shielding lead. Nucl. Instrum. Methods Phys. Res. B 117, 189–198.
Vojtyla, P., 1996b. Influence of shield parameters on cosmic-muon induced backgrounds of Ge γ-spectrometers. Nucl. Instrum. Methods Phys. Res. B 111, 163–170.
Ziegler, J.F., 1996. Terrestrial cosmic rays. IBM J. Res. Dev. 40 (1), 19–39.